Viscous-Inviscid Method for Airfoil Analysis and Design for Aviation and Windmills

Risto Peltonen[*]

Helsinki University of Technology, Laboratory of Aerodynamics, Fin-02015 TKK, Finland

This study examines an advanced viscous-inviscid interactive method developed for the analysis and design of airfoils in two-dimensional subsonic compressible flow ($Ma_\infty < 0.4$). Inviscid flow is solved with a panel method. The laminar boundary layer is calculated by Thwaites' method. Transition is determined by Michel's relation or the e^n method. An integral solution for a turbulent boundary layer is derived from an entrainment equation. Closure conditions are obtained with empirical relations. Singularities near the separation are avoided by inverting the boundary-layer method. Inviscid and viscous flows are coupled with transpiration. The analysis method is used as a "black box" in the design tasks. The geometry of the starting airfoil is perturbed iteratively by transpiration until the pressure distribution converges to a predefined target. This study proposes the necessary degrees of freedom in the target velocity distribution to obtain a closed airfoil. Design cases are included, which support the general applicability and accuracy of the numerical design method.

Nomenclature

c	=	chord length
c_d	=	drag coefficient
C_E	=	entrainment coefficient
C_f	=	skin-friction coefficient based on edge velocity $C_f = 2\tau_w/(\rho u_{iw}^2)$
C_{f0}	=	skin-friction coefficient based on free-stream velocity $C_{f0} = 2\tau_w/(\rho u_\infty^2)$
c_l	=	lift coefficient
c_m	=	pitching-moment coefficient around $0.25c$
C_p	=	pressure coefficient $C_p = 2(p - p_\infty)/\rho U_\infty^2$
H_1	=	velocity-profile form parameter $H_1 = (\delta - \delta_1)/\delta_2$
H_{12}	=	boundary-layer form parameter $H_{12} = \delta_1/\delta_2$
Ma	=	Mach number
$\boldsymbol{n}, \boldsymbol{t}$	=	unit vectors in n, s directions
N	=	number of collocation points
Q	=	total velocity $Q = (u^2 + v^2)^{0.5}$
Re	=	Reynolds number based on chord length $Re = Q_\infty c/\nu$
Re_x	=	Reynolds number based on distance $Re_x = u_{iw}x/\nu$
$Re_{\delta 2}$	=	Reynolds number based on momentum thickness $Re_{\delta 2} = u_{iw}\delta_2/\nu$
s, n	=	curvilinear-streamline dimensionless coordinates ($s = S/c$ and $n = N/c$)
u, v	=	mean flow velocity components in s, n directions
x, y	=	Cartesian dimensionless coordinates ($x = X/c$ and $y = Y/c$)
α	=	angle of attack
β	=	compressibility transformation coefficient $\beta = (1 - Ma_\infty^2)^{0.5}$
γ	=	strength of a vortex; specific-heat ratio
δ	=	boundary-layer thickness
δ_1	=	displacement thickness
δ_2	=	momentum thickness
η	=	distance between singularity surface and airfoil
μ	=	dynamic viscosity
ν	=	kinematic viscosity $\nu = \mu/\rho$
ρ	=	air density
Σ	=	relative blowing velocity $\Sigma = v_{iw}/u_{iw}$
σ	=	strength of a source
τ	=	shear stress; airfoil thickness ratio
Φ	=	velocity potential
ω	=	relaxation parameter

Subscripts/Superscripts

i, I	=	quantity resulting from inviscid calculation
T	=	target
TE	=	trailing edge
U, L	=	upper, lower surface
V	=	quantity resulting from viscous calculation
w, W	=	body wall, wake centerline
$*$	=	incompressible

Introduction

THERE are several different methods for analyzing and designing airfoils, ranging from conformal-mapping techniques[1] to the use of the Navier–Stokes flow solvers. The first mentioned techniques solve inviscid flows whereas the Navier–Stokes flow solvers take the viscosity into account. However, the computation times and costs involved when employing the Navier–Stokes flow solvers, even with the latest generation of supercomputers, remain prohibitive for routine work in the applications of the present study.

The goal is to develop a theoretical model for analyzing and designing two-dimensional single-component airfoils for subsonic flow. The model should include all the necessary viscous and subsonic compressibility effects and should serve sailplane, other general aviation, and wind-turbine applications. In addition, the method should include tools that the designer can use to achieve specific characteristics for the target airfoil.

The methods that predict flows over an airfoil are analysis methods. Relatively few address the design of airfoils, but those that do fall into two categories. The first is the optimization method, where an optimization algorithm iteratively modifies the geometry of the airfoil to maximize the lift coefficient or the glide ratio or minimize the drag coefficient. The second category consists of methods where a potential method is inverted. Theodorsen and Garrick (1933) proposed that Theodorsen's conformal-mapping method[2] could be used in airfoil design by inverting the analysis process. This approach proved possible and led to the development of the laminar low-drag NACA 6-series airfoils. These airfoils were to some extent designed to fit a predefined pressure distribution.

Among the first to propose an exact solution for the inverse problem using conformal mapping were Mangler (1938) and Lighthill

(1945), as noted by Selig and Maughmer.[3,4] They showed that, in the inverse design problem, the surface-pressure distribution and free-stream speed cannot be prescribed independently. The geometry of an airfoil is closed only if the given speed distribution satisfies certain integral constraints.

The inversion of a panel method is usually a rather complicated task. However, the vortex-panel method (Oeller's method) has been inverted successfully for inviscid flows.[5,6] Here, the values of the singularities are obtained directly from the target velocity distribution. Then it is possible to determine the influence coefficients and the airfoil without matrix inversion.

The relation between accuracy and efficiency in viscous-flow predictions is an important factor when selecting a method for analyzing and designing airfoils. In this study, the so-called viscous-inviscid technique is employed. Here, boundary-layer methods for thin shear layers ($\ll$ c) are combined iteratively with potential flow methods for external inviscid flows to provide a composite solution to the problem. The selection is based on the facts: The method is essentially faster than the use of the Navier–Stokes flow solver, provides results nearly as accurate as the Navier–Stokes flow solvers, and presents possibilities to solve the geometry of an airfoil to fit a pre-defined pressure distribution.

In this work, the inviscid method is formulated to include a nonzero normal wall velocity (transpiration), which is a sum of two components: one obtained from the viscous calculations to compensate a boundary layer and a second one needed in design tasks to deform an airfoil. A mild compressibility is taken into account with the Prandtl–Glauert coordinate transformation.

The basic boundary-layer equations (momentum and entrainment) are written into a set of integral equations. For an attached flow, the boundary-layer variables and transpiration velocity are calculated from the pressure distribution obtained from the inviscid calculations. This method is the so-called direct boundary-layer method, which becomes singular at the separation point. In this study, the calculations are then inverted, which means that the pressure distribution and the boundary-layer variables are calculated from the transpiration velocity. A so-called semi-inverse boundary-layer method, proposed by Le Balleur,[7] is applied where the inverse shear-layer calculations are matched with the direct inviscid calculations.

The idea of including the second transpiration component into viscous-inviscid codes has great advantages because it easily converts analysis codes into design codes. The target pressure can be first analyzed with the viscous method so that the aerodynamic properties are acceptable. Then the transpiration component to compensate a displacement thickness can be solved. The target airfoil is then solved by correcting the contour of a starting airfoil by the second component of the transpiration until the viscous-inviscid pressure distribution is close enough to the target. This method is fast, and only a few matrix setups and inversions are needed. The theory described is coded for personal computers. Recently the method has been successfully applied to the investigations of an aircraft accident caused by wing-tip stall.[8]

Geometry Changes by Transpiration

The surface blowing transfers the streamline starting from the stagnation point to a specific distance from the airfoil. This observation, which presents the possibility of changing the geometry of an airfoil without moving the singularity surface, forms the basis for the new design method developed in this study. By correcting the blowing velocity iteratively, it is possible to change the flow pattern so that the pressure distribution becomes equal to a target pressure. A curvilinear rectangular coordinate system (s, n) is fixed on the starting airfoil. The target airfoil can be expressed in the same coordinate system by adding a displacement in the n direction to the airfoil (Fig. 1),

$$\eta = \eta(s) \tag{1}$$

With the surface correction η given, the displacement thickness δ_1 obtained from the boundary-layer equations, and tangential velocity
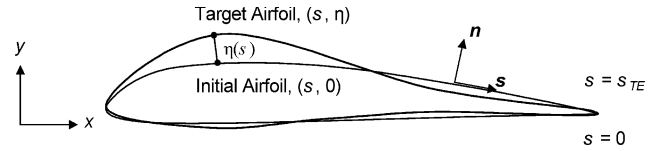

Fig. 1 Target airfoil expressed by adding a displacement $\eta(s)$ in the n direction to the initial airfoil.

u obtained from the inviscid method, the normal velocity v has the following expression in the design code:

$$v = \frac{1}{\rho} \frac{d}{ds}[\rho u(\delta_1 + \eta)] = v_{iw} + v_\eta \tag{2}$$

In the analysis mode η (and v_η) is set to zero.

Panel Method

In the present study, the singularity combination has a piecewise, constant-strength distribution of sources and vortices along straight-line panels. The method includes wake effects and a mild compressibility ($Ma_\infty < 0.4$) by the Prandtl–Glauert coordinate transformation. The vortex distribution around the airfoil can be constant ($\xi = 1$) or a parabolic distribution,

$$\xi(x) = \sqrt{1 - x}, \qquad 0 \le x \le 1 \tag{3}$$

Singularities are distributed over each of N panels along the surface of the airfoil and N_w panels along the wake-dividing streamline. The resulting system of linear equations for normal velocities at the panels on the airfoil reads as follows:

$$v_i = \sum_{j=1}^{N} a_{ij}\sigma_j + \gamma \sum_{j=1}^{N} b_{ij}\xi_j + \boldsymbol{Q}_{ef_i} \cdot \boldsymbol{n}_i \tag{4}$$

or

$$[a][X] = [R] \qquad \text{or} \qquad \sum_{j=1}^{N+1} a_{ij}X_i = R_j \tag{5}$$

The matrix $[a]$ contains normal velocity influence coefficients. In the vector $[R] = [-\boldsymbol{Q}_{ef} \cdot \boldsymbol{n} + v]$, the effective freestream velocity $\boldsymbol{Q}_{ef}$ is sums of the constant free-stream velocity $\boldsymbol{Q}_\infty$ and the velocity induced by the singularities of the wake. The system is closed via the Kutta condition of equal tangential velocities at the trailing edge.

The calculation of the unknown singularities on the airfoil $[X] = [\sigma_j, \gamma]$ is reduced to

$$[X] = [a]^{-1}[R] \qquad \text{or} \qquad X_i = \sum_{j=1}^{N+1} a_{ij}^{-1} R_j \tag{6}$$

where the a_{ij}^{-1} are the elements of the inverted matrix $[a]$. In the wake sink and vortex, distributions are obtained using the viscous method and the definitions for normal and tangential velocity jumps:

$$\sigma = \langle v_W \rangle = \Sigma_{U,L} \frac{1}{\rho_{iW}} \frac{d}{ds}(\rho_{iW} u_{iW}\delta_1) \tag{7}$$

$$\gamma = \langle u_W \rangle = \Sigma_{U,L} - k u_{iW}(\delta_1 + \delta_2) \tag{8}$$

The curvature of the wake is determined by the curvature of the wake center, which is defined as the radius or using (x, y) coordinates of the streamline starting from the trailing edge:

$$k_W = \frac{1}{r} \approx \frac{d^2 y}{dx^2} \tag{9}$$

Tangential velocity distribution on the airfoil and in the wake-dividing streamline is obtained by summing the effects of the singularities and the free-stream velocity:

$$u_i = \sum_{j=1}^{N} \sigma_j A_{ij} + \gamma \sum_{j=1}^{N} \xi_j B_{ij} + \sum_{k=1}^{N_W} \sigma_k A_{ik} + \sum_{k=1}^{N_W} \gamma_k B_{ik} + Q_{\infty t} \tag{10}$$

Here A and B are tangential-influence coefficients of the singularities on the airfoil and in the wake.

If the shape of the singularity surface remains unchanged, then the influence matrix setup and inversion occurs only once and the inviscid part of the calculations is reduced to Eqs. (6) and (10). Avoiding subsequent matrix operations is a significant point in favor of iterative-calculation economy, because the matrix setup and inversion of influence coefficients are the most time-consuming procedures in the panel methods.

If $\xi(s) = 1$, an unrealistic pressure loop is found near a cusped or thin trailing edge of an airfoil. This problem has been demonstrated in Ref. 9. The loss of accuracy results from the vortex influence of opposite panels that may be close to each other. This inaccuracy can be removed using a parabolic vortex distribution so that the vortex disappears at the trailing edge.

Integral Relations for Boundary Layers and Wakes

An important computational requirement is the capability to accurately represent flows with a limited trailing-edge separation region. A transition with a possible separation bubble should be represented analytically in a continuous manner. Computational economy, meaning as few viscous variables as possible, is very important in the global solution procedure. To meet these requirements, the viscous flow calculation is based on the solution of integral equations for a compressible boundary layer. The tangential velocity distribution calculated with the panel method is transferred to the boundary-layer procedures through the definition u_{iw}. The transpiration-velocity component compensating the boundary layer is denoted with v_{iw}.

Laminar Boundary Layer and Transition

For the laminar part of the boundary layer, the momentum thickness is solved by Thwaites' method[10,11]:

$$\delta_2^2(s) = \frac{0.45}{Re\, u_{iw}^6} \int_0^s u_{iw}^5 \, ds \tag{11}$$

Then the empirical closure relations give information on the shape factor H_{12} and skin friction C_f. The compressible correction is done as proposed by Cohen and Reshotko.[12] Thwaites' method is fairly accurate, but as a single-equation method it cannot describe separated flow regions.

In the decelerating flow, laminar separation is deduced from a velocity-gradient parameter λ (Ref. 11):

$$\lambda = Re\, \delta_2^2 \frac{du_{iw}}{ds} \tag{12}$$

Laminar separation is expected to occur at a location s where $\lambda(s) \leq -0.09$. Two alternative criteria are used to predict the natural transition point.

The e^n Method

A boundary layer will be initially laminar and will become unstable at the point s_{Cr} where undamped Tollmien–Schlichting waves first appear. These waves will grow and distort until the point of transition, or fully turbulent flow, is reached. A transition prediction assumes that the transition occurs when the amplitude of the most unstable Tollmien–Schlichting wave in the boundary layer has grown by some factor, usually taken to be $A/A_0 = e^{10} \approx 22{,}000$.

The empirical relations by Drela and Giles[13] are easy to implement in Thwaites' method. The natural logarithm of the maximum amplification ratio is denoted by n, and it is related to the local

boundary-layer parameters H_{12} and $Re_{\delta 2}$. The laminar boundary layer becomes unstable when the local Reynolds number based on the momentum thickness $Re_{\delta 2}$ exceeds the critical value $Re_{\delta 2Cr}$ expressed by the empirical formula:

$$\log_{10} Re_{\delta 2cr} = \left(\frac{1.415}{H_{12}-1} - 0.489 \right) \tanh\left(\frac{20}{H_{12}-1} - 12.9 \right)$$
$$+ \frac{3.295}{H_{12}-1} + 0.44 \tag{13}$$

Then the transition point is determined by integrating the local amplification rate downstream from the point of instability s_{Cr}

$$n(s) = \int_{s_{Cr}}^{s} \frac{dn}{ds} \, ds \tag{14}$$

The spatial amplification rate with respect to the streamwise coordinate s from the stagnation point is determined as

$$\frac{dn}{ds} = \frac{dn}{dRe_{\delta 2}} \frac{dRe_{\delta 2}}{ds} = \frac{dn}{dRe_{\delta 2}} \frac{1}{2} \left(\frac{s}{u_{iw}} \frac{du_{iw}}{ds} + 1 \right) \frac{\rho_{iw} u_{iw} \delta_2^2}{\mu_{iw} s} \frac{1}{\delta_2} \tag{15}$$

Using the empirical formulas

$$\frac{dn}{dRe_{\delta 2}}$$
$$= 0.01\sqrt{[2.4 H_{12} - 3.7 + 2.5 \tanh(1.5 H_{12} - 4.65)]^2 + 0.25} \tag{16}$$

$$\frac{\rho_{iw} u_{iw} \delta_2^2}{\mu_{iw} s} = l(H_{12}) = \frac{6.54 H_{12} - 14.07}{H_{12}^2} \tag{17}$$

$$\frac{s}{u_{iw}} \frac{du_{iw}}{ds} = m(H_{12}) = \left(0.058 \frac{(H_{12}-4)^2}{H_{12}-1} - 0.068 \right) \frac{1}{l(H_{12})} \tag{18}$$

the amplification rate with respect to s is expressed as a function of H_{12} and δ_2:

$$\frac{dn}{ds}(H_{12}, \delta_2) = \frac{dn}{dRe_{\delta 2}}(H_{12}) \frac{m(H_{12})+1}{2} l(H_{12}) \frac{1}{\delta_2} \tag{19}$$

The transition is assumed to occur when $n(s)$ in Eq. (14) reaches a critical value (usually from 9 to 12).

Michel's Empirical Criterion

A relation[11] is used to predict the transition-point location. The transition is supposed to take place when

$$Re_{\delta 2} > 1.174 \left(1 + \frac{22{,}400}{Re_s} \right) Re_s^{0.46} \tag{20}$$

where Re_s is the Reynolds number based on the distance s from the stagnation point.

On each side of the airfoil, a transition point is defined nearest to the stagnation point as allowed by one of the following: laminar separation predicted by Thwaites' method, transition predicted by e^n or Michel's method, or user-defined point of transition.

Turbulent Boundary Layer for Attached Flow

The integral equations for a turbulent boundary layer usually comprise one equation for the momentum thickness, Eq. (21). Because the interaction between δ_2, H_{12}, and C_f is far more complicated than in laminar flow, independent relations are needed to achieve a closed system of boundary-layer equations. A characteristic of multiequation methods is that, if properly formulated, they in principle can describe thin, separated regions.

In this study, the approach used is the concept of entrainment,[11] originally introduced by Head and later extended and improved

by Green et al.[14] Various modifications to improve its applicability under separated flow conditions have been used as the technical foundation of this work.[15,16]

The entrainment-integral relationship is derived from Head's assumption that turbulent boundary layers grow by a process of entrainment from the free stream into the boundary layers of nonturbulent flow at the outer edge of the layer. The entrainment into the boundary layer depends on the velocity defect in the outer part of the layer and is independent of viscosity. Closure relations are defined with parameters such as the skin friction and form parameter. This combination of the basic equations is taken from Green's method. The boundary-layer equations for attached flows are listed next.

Differential Equation for Momentum Thickness

$$\frac{d\delta_2}{ds} = \frac{1}{2}C_f - \left(H_{12} + 2 - Ma_{iw}^2\right)\frac{\delta_2}{u_{iw}}\frac{du_{iw}}{ds} \qquad (21)$$

Differential Equation for Form Parameter H_{12}^*

The entrainment coefficient defined by

$$C_E = \frac{1}{\rho_e u}\frac{d}{ds}\int_0^\delta \rho u\, dn = \frac{1}{\rho_{iw}u_{iw}}\frac{d}{ds}[\rho_{iw}u_{iw}(\delta - \delta_1)] \qquad (22)$$

is the (dimensionless) rate at which fluid from the external inviscid flow enters through the outer edge of the boundary layer. By defining an entrainment form parameter by the formula $H_1 = (\delta - \delta_1)/\delta_2$, Eq. (22) becomes

$$C_E = H_1\frac{d\delta_2}{ds} + H_1\left(1 - Ma_{iw}^2\right)\frac{\delta_2}{u_{iw}}\frac{du_{iw}}{ds} + \delta_2\frac{dH_1}{ds} \qquad (23)$$

By combining Eqs. (21) and (23) and using the form-parameter definition H_{12}, the following second boundary-layer equation is obtained:

$$\frac{dH_{12}^*}{ds} = \frac{1}{\delta_2}\frac{dH_{12}^*}{dH_1}\left\{C_E - H_1\left[0.5C_f - (H_{12}+1)\frac{\delta_2}{u_{iw}}\frac{du_{iw}}{ds}\right]\right\} \qquad (24)$$

For a compressible flow H_{12}^* (in any previous form) should be replaced by the transformed form parameter H_{12}:

$$H_{12}^* = \frac{\delta_1^*}{\delta_2} = \frac{1}{\delta_2}\frac{1}{\rho_{iw}u_{iw}}\int_0^\delta \rho(u_i - u)\, dn \qquad (25)$$

With zero wall-heat transfer, the relation is[14]

$$H_{12} = (H_{12}^* + 1)\left(1 + \tfrac{1}{5}Ma_{iw}^2\right) - 1 \qquad (26)$$

The two basic differential equations (21) and (24) contain three variables, u_{iw}, H_{12}^*, and δ_2. The direct formulation corresponds to a solution with a prescribed velocity distribution u_{iw}.

Closure Conditions

Before the basic differential equations can be solved, additional unknowns must be specified by further assumptions (closure conditions) that are empirical and theoretical. The following functional dependencies are assumed:

1) The entrainment coefficient is a function of H_1, $C_E = G(H_1)$ (Ref. 17):

$$C_E = \lambda 0.0306(H_1 - 1)^{-0.6169} \qquad (27)$$

with extension $\lambda = 1$ on the airfoil and $\lambda = 2$ in the wake.

2) The entrainment form parameter H_1 is in turn a function of H_{12}^*; that is, $H_1 = F(H_{12}^*)$:

$$H_1 = \begin{cases} \dfrac{0.63H_{12}^{*2} + H_{12}^*}{H_{12}^* - 1} - 0.65, & H_{12}^* < 2.60851 \\[2ex] 4.0 + \dfrac{a_1}{H_{12}^* + a_2} + \dfrac{a_3}{H_{12}^*}, & H_{12}^* \geq 2.60851 \end{cases} \qquad (28)$$

3) The local skin-friction coefficient C_f is a function of the form parameter H_{12}^*, the Reynolds number based on momentum thickness $Re_{\delta 2}$, and the local Mach number Ma_{iw}. The relation is

$$F_c C_f = 0.3e^{-1.33H_{12}^*}\left(\log_{10}\frac{Re_{\delta 2}}{F_c}\right)^{-1.74 - 0.31H_{12}^*}$$

$$+ 1.1 \times 10^{-4}\left[\tanh\left(4 - \frac{H_{12}^*}{0.875}\right) - 1\right] \qquad (29)$$

with

$$F_c = 1 + \tfrac{1}{5}Ma_{iw}^2 \qquad (30)$$

Many closely related alternatives have been proposed for the form parameter H_1 (Refs. 18–22). In this study, Eq. (28) has been developed to describe both the attached and separated flow regions using an empirical approach supported by experimental data published in Ref. 23. When $H_{12}^* < 2.60851$, a curve-fitting technique and numerical tests are used to define the constants. The pressure distribution has been found realistic and nearly constant in highly separated flows when H_1 approaches asymptotically the value 4.0. In the case of $H_{12}^* \geq 2.60851$, the coefficients a_1, a_2, and a_3 are found from a smooth-matching condition so that the form parameter H_1 is continuous at $H_{12}^* = 2.60851$ up to the second derivative. The coefficients are $a_1 = 0.02039$, $a_2 = -2.25293$, and $a_3 = -1.09717$.

The skin-friction coefficient is taken from the work of Swafford,[24] which gives $C_f < 0$ when the flow is separated.

The uncertainties in the definition of H_1, together with similar problems regarding the calculation of C_E, represent the chief limitations to entrainment methods. Unfortunately, it is unlikely that any unique (H_{12}^*, H_1) and (H_1, C_E) relationship can be found that is valid for all cases of practical interest. However, the main numerical results of such methods (values of δ_1, δ_2, and C_f, for example) are not unduly sensitive to either of these features, which explains their general success in a wide variety of cases.

Initial data for turbulent flow is specified at the transition or reattachment point. It is assumed that the momentum thickness is continuous in a natural transition, and the initial turbulent value of δ_2 is taken from the laminar calculations.

Transition Strip

If the transition point is specified by input, a simple transition strip-modeling by Michel and Arnal.[25] is incorporated, which increases the momentum thickness by

$$\Delta \delta_{2\text{Tr}} = 0.5C_D\left(\frac{u(h)}{u_{iw}}\right)^2 h \qquad (31)$$

Here h is the height of the transition strip, and $u(h)$ is the velocity in the laminar boundary layer without the transition strip at $n = h$. It appears that high turbulence intensities are not created on the roughness itself but rather in a separated region downstream. In an ideal case, the transition strip has a height that only fixes the transition without additional drag. However, the height of the transition strip is usually more than that needed to cause a transition. Experimental tests show that C_D is usually close to 0.4 but increases up to 0.6 when the roughness height is greater than the boundary-layer thickness.

Inverting Viscous Calculations

The function $H_1 = F(H_{12}^*)$ has a minimum at $H_{12}^* \approx 2.6$, and here the derivative dH_{12}^*/dH_1 becomes infinite. Near the minimum, high values of the derivative increases the error in the second basic differential equation (24). The singular point can be avoided by solving in an inverse manner, in which Σ is specific and du_{iw}/ds is unknown. The relative blowing velocity can be calculated from the equation

$$\Sigma = \frac{1}{\rho_{iw}u_{iw}}\frac{d}{ds}(\rho_{iw}u_{iw}H_{12}\delta_2) = H_{12}\frac{d\delta_2}{ds}$$

$$+ H_{12}\left(1 - Ma_{iw}^2\right)\frac{\delta_2}{u_{iw}}\frac{du_{iw}}{ds} + \delta_2\frac{dH_{12}}{ds} \qquad (32)$$

To eliminate $\mathrm{d}H_{12}/\mathrm{d}s$ from Eq. (24), we first differentiate Eq. (26), using the derivative

$$\frac{\mathrm{d}Ma_{iw}^2}{\mathrm{d}s} = 2Ma_{iw}^2\left[1 + \frac{1}{2}(\gamma - 1)Ma_{iw}^2\right]\frac{1}{u_{iw}}\frac{\mathrm{d}u_{iw}}{\mathrm{d}s} \quad (33)$$

to obtain ($\gamma = 1.4$)

$$\frac{\mathrm{d}H_{12}}{\mathrm{d}s} = \left(1 + \frac{1}{5}Ma_{iw}^2\right)\frac{\mathrm{d}H_{12}^*}{\mathrm{d}s} + \frac{2}{5}Ma_{iw}^2(H_{12} + 1)\frac{1}{u_{iw}}\frac{\mathrm{d}u_{iw}}{\mathrm{d}s} \quad (34)$$

The three equations (21), (23), and (32) can be written in matrix form as

$$
\begin{pmatrix}
1 & H_{12} + 2 - Ma_{iw}^2 & 0 \\
H_1 & H_1\left(1 - Ma_{iw}^2\right) & H_1' \\
H_{12} & H_{12} + \frac{1}{5}Ma_{iw}^2(2 - 3H_{12}) & 1 + \frac{1}{5}Ma_{iw}^2
\end{pmatrix}
\begin{pmatrix}
\dfrac{\mathrm{d}\delta_2}{\mathrm{d}s} \\[2mm]
\dfrac{\delta_2}{u_{iw}}\dfrac{\mathrm{d}u_{iw}}{\mathrm{d}s} \\[2mm]
\delta_2\dfrac{\mathrm{d}H_{12}^*}{\mathrm{d}s}
\end{pmatrix}
$$

$$
= \begin{pmatrix} 0.5C_f \\ C_E \\ \Sigma \end{pmatrix} \quad (35)
$$

where $H_1' = \mathrm{d}H_1/\mathrm{d}H_{12}^*$. These equations can be solved to give the momentum thickness, velocity, and form parameter.

Momentum Thickness

$$(H_{12} + 1)D\frac{\mathrm{d}\delta_2}{\mathrm{d}s} = (H_{12} + 2 - Ma_{iw}^2)\left\{C_E\left(1 + \frac{1}{5}Ma_{iw}^2\right)\right.$$

$$\left. - \Sigma H_1'\right\} - 0.5C_f\left\{H_1 - H_{12}H_1' - \frac{1}{5}Ma_{iw}^2\left(4H_1 + 2H_1'\right.\right.$$

$$\left.\left. - 3H_{12}H_1'\right) - \frac{1}{5}Ma_{iw}^4H_1\right\} \quad (36)$$

Velocity

$$(H_{12} + 1)D\frac{\delta_2}{u_{iw}}\frac{\mathrm{d}u_{iw}}{\mathrm{d}s} = \Sigma H_1' + 0.5C_f\left\{\left(1 + \frac{1}{5}Ma_{iw}^2\right)H_1\right.$$

$$\left. - H_{12}H_1'\right\} - C_E\left(1 + \frac{1}{5}Ma_{iw}^2\right) \quad (37)$$

Form Parameter

$$D\delta_2\frac{\mathrm{d}H_{12}^*}{\mathrm{d}s} = \Sigma H_1 - \frac{1}{5}Ma_{iw}^2H_1C_f - C_E\left(H_{12} - \frac{2}{5}Ma_{iw}^2\right) \quad (38)$$

The inverted equations contain a parameter

$$D = \left(\tfrac{2}{5}Ma_{iw}^2 - H_{12}\right)H_1' + \left(1 + \tfrac{1}{5}Ma_{iw}^2\right)H_1 \quad (39)$$

If the flow is highly separated ($H_{12} > 5$), then approximations $H_1' \approx 0$, $C_f \approx 0$, and $H_1 \gg C_E$ reduce the velocity equation (37) to the form

$$(H_{12} + 1)\frac{\delta_2}{u_{iw}}\frac{\mathrm{d}u_{iw}}{\mathrm{d}s} \approx 0.5C_f - \frac{C_E}{H_1} \approx 0 \quad (40)$$

This results in a nearly constant velocity distribution, which has been observed in wind-tunnel tests for separated flows. Switching to the inverted equations (36–38), when $H_{12}^* > 1.9$, the parameter

D can never vanish and thus the inverted boundary-layer equations are nonsingular. The three equations are integrated simultaneously, similar to the treatment of the direct equations. The inverse method predicts a velocity distribution u_{iw}, δ_2, and H_{12}^* from a given relative blowing-velocity distribution Σ.

Viscous-Inviscid Matching Procedure

Direct Matching

In attached flows, the classical direct matching scheme is used. For a turbulent boundary layer, the user can select an initial value of H_{12}^*. For natural transition, the starting value is found in experiments usually to be 1.3 to 1.6, and when a separation bubble or a transition strip exists, a value of about 1.8 is found.[25] The form parameter of turbulent flow lies in a rather narrow range in a slight pressure gradient. The boundary-layer parameters soon find their equilibrium values that do not depend on the initial values.

On the airfoil, the boundary-layer equations are integrated simultaneously using a fourth-order Runge–Kutta method,[26] with the same calculation grid as in the panel method. The boundary-layer calculations are continued downstream from the trailing edge with $C_f = 0$. Both sides of the wake are calculated separately using the inviscid velocity u_{iW} on the dividing streamline. The drag coefficient c_d converges when the length of the wake is about 10 chords. The momentum thickness is continuous at the trailing edge, but the trailing edge thickness h_{TE} is added to the initial values of the displacement thicknesses.

The blowing velocity is relaxed using the difference between the computed $v_{iw}^{(n+1)}$ and the previous $v_{iw}^{(n)}$ blowing velocity

$$v_{iw}^{(n+1)} = v_{iw}^{(n)} + \omega_1\beta\left(v_{iw}^{(n+1)} - v_{iw}^{(n)}\right) \quad (41)$$

The direct matching can always be stabilized by underrelaxation ($\omega_1 = 0.1 - 0.3$) and it usually converges quickly.

Semi-Inverse Matching

From the beginning of the inverse boundary-layer solution, the relative blowing velocity

$$\Sigma = \frac{v_{iw}}{u_{iw}} = \frac{1}{\rho_{iw}u_{iw}}\frac{d}{ds}(\rho_{iw}u_{iw}H_{12}\delta_2) \quad (42)$$

is updated by the relaxation formula

$$\Sigma^{(n+1)} = \Sigma^{(n)} + \omega_2\beta\Delta s\left(\frac{1}{u_{iw}^{(V)}}\frac{\mathrm{d}u_{iw}^{(V)}}{\mathrm{d}s} - \frac{1}{u_{iw}^{(I)}}\frac{\mathrm{d}u_{iw}^{(I)}}{\mathrm{d}s}\right) \quad (43)$$

Here, $u_{iw}^{(V)}$ is the velocity obtained by the inverse method, and $u_{iw}^{(I)}$ is the velocity obtained from the inviscid calculations (panel method). The factor ω_2 can be selected to be from 1.0 to 2.5, and Δs is the local panel length.

The inverse boundary-layer calculation continues into and along the wake (taking account of possible nonzero trailing-edge thickness) until the value of H_{12}^* drops below the switch value of 1.9. Then the direct method is adopted again.

Drag Coefficient

The computer program contains three known methods for defining the drag coefficient:

1) One is from the flow far downstream

$$c_d = 2\delta_{2\infty}/c \quad (44)$$

where $\delta_{2\infty}$ is the momentum thickness at the end of the wake calculations.

2) The second is from the flow at the trailing edge with a modified Squire–Young formula[27,28]:

$$c_d = 2\delta_{2TE}u_{iw}^{(\overline{H_{12TE}}+5)/2}, \qquad \overline{H_{12TE}} = \mathrm{Min}(H_{12TE}, 2.5) \quad (45)$$

The drag coefficient is the sum of the values calculated separately for the upper and lower surfaces.

3) The third is integrated drag coefficient from the surface-pressure and skin-friction distributions.

Convergence Criteria

The calculation cycle in the analysis or design mode is repeated until the following typical convergence limits are reached between two successive iterations: 1) change in lift coefficient $|\Delta c_l| < 0.001$ and 2) change in trailing-edge pressure coefficient $|\Delta C_p| < 0.005$.

In the analysis mode, the difference between the direct and inverse velocity distributions fulfils

$$\Delta u = \int_0^{s_{TE}} \left| u_{iw}^{(I)} - u_{iw}^{(V)} \right| ds < 0.01 \qquad (46)$$

In the design mode the difference between the obtained and target velocity distribution fulfils

$$\Delta u = \int_0^{s_{TE}} |u_{iw} - u_r| ds < 0.015 \qquad (47)$$

Design of Airfoils

The problem of designing airfoils has been a subject of considerable theoretical interest for more than half a century. The aerodynamic performance of an aircraft (wind generator, F1 car, etc.) can be greatly enhanced by tailoring the airfoil to its specific requirements. A slight drag decrease of a big transport aircraft may result in remarkable fuel savings in a year. Many boundary conditions and requirements should be taken into account, some of which conflict with each other. For example, a sailplane or windmill wing profile should have the following characteristics: low drag and moment coefficient, and high maximum lift coefficient, lift-to-drag ratio (c_l/c_d), and power factor ($c_l^{1.5}/c_d$). Stalling should be smooth without sensitivity to surface roughness. The profile should be thick enough for structural reasons.

An inverse problem is to find a geometry that satisfies some pressure or velocity distribution that provides the required behavior of a boundary layer to give high lift and low drag coefficient. Originally it was solved for potential flows (conformal mapping), but currently viscous effects can be taken into account using viscous-inviscid methods, as in the present study or the Navier–Stokes equations.

If a viscous integral-boundary-layer method is used, the aerodynamic coefficients can be defined from the target pressure distribution without solving for the airfoil, as is shown in this work. If the target pressure has the desired characteristics, the corresponding airfoil coordinates are then solved, usually by interactive calculations.

The problem is in general not well posed, unless the specific speed distribution satisfies certain constraints. Any prescribed viscous pressure distribution will not necessarily imply a closed practical airfoil. Therefore, the pressure distribution must be checked by determining the geometry of the airfoil. A good design code should have free parameters to modify the target pressure distribution or the resulting airfoil. In practice, the modifications are reduced to a variation of the trailing-edge velocity and a slight bending of the airfoil contour to close the geometry.

Using an Analysis Code in Airfoil Design

It is quite often impossible to fully invert an analysis code. Semi-inverse design methods are quite popular because every analysis code or a part of it (e.g., influence coefficients) can be used. Here the inverse problem is nonlinear and the unknown surface is solved iteratively.

In this study, a Neumann-type residual-correction design method is selected. The main advantage is its simplicity. In principle, every analysis code can be used without modifications, but those using surface transpiration to represent viscous effects are preferred. Because transpiration can also be used to modify the airfoil contour, the number of mesh-correction operations can be considerably limited.

The analysis code is retained in its original form and can be treated solely as a "black box." The same viscous and compressible effects that occur in the analysis tasks can be included in the airfoil design.

Efforts can be concentrated on coding an inverse routine, based on a suitable approach, and on coupling the routine to the analysis code. The analysis code can easily be replaced with a more advanced code when one becomes available.

Semi-Inverse Residual-Correction Method

Basic Equations

In this study, the geometry of an airfoil is corrected in the first stage by transpiration. The target velocity distribution is denoted by u_T. The calculations are organized in a design task as follows: the boundary layer and blowing velocity v_{iw} are solved from the selected target velocity distribution u_T, and the analysis code will calculate the tangential velocity distribution u when the blowing velocity v is detected as Eq. (2):

$$v = \frac{1}{\rho} \frac{d}{ds} [\rho u_T (\delta_1 + \eta)] = v_{iw} + v_\eta \qquad (48)$$

A correction algorithm is needed, which defines η from the difference between the target u_T and actual u_{iw} velocity distribution. The final aerodynamic shape is approached in a stepwise fashion through a cyclic iteration between the viscous-inviscid flow solver and airfoil geometry corrector. The airfoil is found when the target and actual velocities become identical. In this study, an auxiliary partial differential equation is proposed that is solved for a geometry correction of a surface during each design cycle.

The pressure distribution is assumed to be a function of the thickness, slope, and curvature of the airfoil and free-stream conditions. With these assumptions, Garabedian and McFadden[29] have developed a corrector that is a second-order differential equation. Also Malone et al.[30,31] have used the same formula in a semi-inverse Navier–Stokes design method.

In this study, the pressure distribution is taken to be a function of the y-coordinate of the profile except near the trailing edge where it is a function of the slope of the contour. The following first-order differential equation is obtained:

$$\eta + K \frac{d\eta}{ds} = R \qquad (49)$$

Near the trailing edge ($x \geq 0.95c$) on the suction side [$q_t(s) > 0$] the constant K equals 1, and on the pressure side [$q_t(s) < 0$] K equals -1. Otherwise ($x < 0.95c$) K is set to 0. The pressure (velocity) residual R is

$$R = \Delta s \begin{cases} \omega_1 \left(u_T^2 - u_{iw}^2 \right), & x(s) < 0.95c \\ \omega_2 \left(\dfrac{1}{u_T} \dfrac{du_T}{ds} - \dfrac{1}{u_{iw}} \dfrac{du_{iw}}{ds} \right), & x(s) \geq 0.95c \end{cases} \qquad (50)$$

The relaxation coefficients $\omega_{1,2}$ are selected from 0.1 to 0.4 to provide a stable iterative process, and Δs_i is the length of panel i. Equation (49) is written for the correction $\Delta \eta$ to the coordinates as

$$\Delta \eta + K(\Delta \eta)_s = R \qquad (51)$$

The computational grid is still the same as in the analysis. Around the initial airfoil ($0 \leq s \leq s_{TE}$) at each control point (panel midpoint) $P_i, i = 1, \ldots, N$, Eq. (51) is discretized by the central-difference approximation

$$\Delta \eta_i + K \frac{\Delta \eta_{i+1} - \Delta \eta_{i-1}}{s_{i+1} - s_{i-1}} = R_i, \qquad i = 2, \ldots, N-1 \quad (52)$$

A forward- and backward-difference approximation is used for the endpoints

$$\Delta \eta_1 + K \frac{\Delta \eta_2 - \Delta \eta_1}{s_2 - s_1} = R_1 \qquad (53)$$

$$\Delta \eta_N + K \frac{\Delta \eta_N - \Delta \eta_{N-1}}{s_N - s_{N-1}} = R_N \qquad (54)$$

A typical equation evaluated at the ith point on the initial surface is

$$A_i \Delta \eta_{i+1} + B_i \Delta \eta_i + C_i \Delta \eta_{i-1} = R_i \qquad (55)$$

The following expressions are obtained for the coefficients:

$$A_N = 1 + \frac{K}{s_N - s_{N-1}}, \qquad B_N = -\frac{K}{s_N - s_{N-1}} \qquad (56)$$

$$A_i = \frac{K}{s_{n+1} - s_{n-1}}, \qquad B_i = 1,$$

$$C_i = -\frac{K}{s_{n+1} - s_{n-1}}, \qquad N = 2, \dots, N-1 \qquad (57)$$

The algebraic Eqs. (55) form a tridiagonal system, which is solved for values of $\Delta \eta_i$ with the Thomas algorithm[26]:

$$
\begin{pmatrix}
B_1 & C_1 & & & & \\
A_2 & B_2 & C_2 & & & \\
& A_3 & B_3 & C_3 & & \\
& \dots & \dots & \dots & & \\
& & A_{n-1} & B_{N-1} & C_{N-1} & \\
& & & & A_N & B_N
\end{pmatrix}
\begin{pmatrix}
\Delta \eta_1 \\
\Delta \eta_2 \\
\Delta \eta_3 \\
\dots \\
\Delta \eta_{N-1} \\
\Delta \eta_N
\end{pmatrix}
$$

$$
=
\begin{pmatrix}
R_1 \\
R_2 \\
R_3 \\
\dots \\
R_{N-1} \\
R_N
\end{pmatrix}
\qquad (58)
$$

The inverse problem can be solved by the iteration process as follows:

1) When the starting airfoil is selected, the initial guess for airfoil correction in the normal direction is set to $\eta(s)^{(1)} = 0$.

2) Using the boundary-layer procedure, the displacement thickness δ_1 is calculated from the target velocity distribution u_T. If this flow is attached ($H_{12}^* < 1.9$), only one direct boundary-layer calculation is needed on the airfoil. In the wake, the iterative direct or inverse boundary-layer procedure is repeated as part of the design cycle.

3) The new blowing velocity $v = v_{iw} + v_\eta$, compensating the boundary layer and correcting the geometry, is obtained from Eq. (47). Using v as input, a pressure distribution is calculated by the inviscid method including the viscous and wake effects on the initial airfoil as in the analysis mode.

4) The local residuals R_i are determined from Eq. (50) and the tridiagonal system Eq. (58) is solved for the incremental change in the surface coordinates $\Delta \eta_i$.

5) At the end of the design cycle, the displacement for the initial airfoil $\eta_i^{(n+1)}$ is updated as follows:

$$\eta_i^{(n+1)} = \eta_i^{(n)} + \Delta \eta_i, \qquad i = 1, \dots, N \qquad (59)$$

The design procedure is repeated until the local residuals R_i in Eq. (58) disappear and the calculated velocity u_{iw} and target velocity u_T distributions are equal within the tolerance limits.

Defining the Coordinates

The initial airfoil $(x_i, y_i), i = 1, \dots, N+1$, is stretched in the normal direction (Fig. 2). The coordinates of the target airfoil are

$$(x_i, y_i)^{(n+1)} = (x_i, y_i) + 0.5 \left(\eta_{i-1}^{(n+1)} + \eta_i^{(n+1)} \right) (n_x, n_y)_i \qquad (60)$$

Here $(n_x, n_y)_i$ are the scalar components of the normal unit vectors $\mathbf{n}_i^\circ$ on the contour. Finally, the coordinates are normalized so that the leading edge is tangential to the y-axis and at the trailing edge $x = 1$.
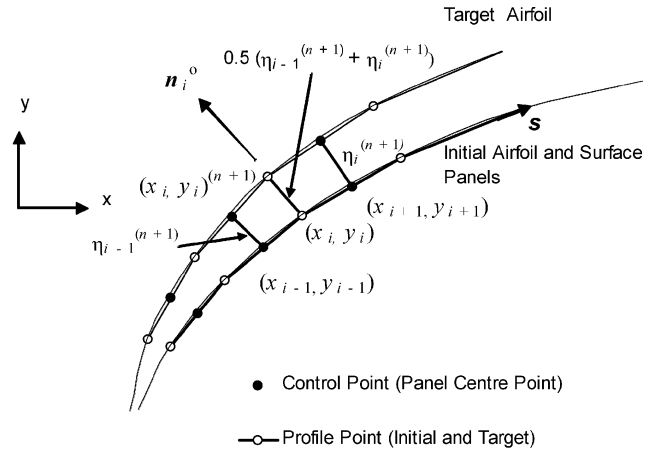

Fig. 2 Initial airfoil is stretched in the normal direction to obtain the target airfoil.

Trailing-Edge Closure

An airfoil determined for an arbitrary pressure distribution has an open trailing edge or crossed surfaces. For viscous flows there are no analytical constraints to guarantee a closed solution (or a particular trailing-edge thickness). This indicates that a specified surface-velocity distribution has to be altered in such a manner as to satisfy the geometrical requirements. Usually the ideal speed distribution is modified over selected segments of the airfoil surface. The desired characteristic of a velocity (e.g., "rooftops," Wortmann-type pressure recovery, rear or front loading) can be retained with little or no modification. The target pressure can be corrected by the following methods.

1) Using feedback from the resulting airfoil, the target trailing-edge velocity is corrected manually, which affects the velocity gradient in the turbulent flow. If the airfoil chord tends to rotate, the initial angle of attack may be corrected at the same time.

2) The final trailing-edge closure is obtained by rotating the airfoil contours around the leading edge. If Δ is the trailing-edge thickness obtained and Δ_T is the target value, the rotated y-coordinates for the upper and lower surfaces are, respectively,

$$y_{u,l}(x) = y_{u,l}(x)^{(n+1)} \pm 0.5(\Delta_T - \Delta)(x/c) \qquad (61)$$

Usually 5 to 20 transpiration iteration cycles result in convergence. The geometry obtained is then the new initial airfoil. About 3 to 15 target-pressure corrections and matrix inversions are needed to obtain a sufficiently accurate result.

Target Velocity-Distribution Equations

The pressure levels of the upper and lower surfaces are determined by the lift coefficient. To cover all the viscous effects, a laminar-turbulent transition is implemented in the predefined pressure distribution. There is no need to define the geometry of an airfoil at first. Because there are two separate modules in the iterative viscous-inviscid methods, the viscous characteristics of the target velocity distribution can be analyzed first.

On the upper and lower sides of an airfoil, the velocity distribution is divided into five regions. These regions are illustrated schematically in Fig. 3.

Stagnation Region

After the initial airfoil has been selected, the analysis code calculates its inviscid pressure distribution and the stagnation point. About 1.5% of the calculated velocity distribution downstream from the stagnation point on both sides of the airfoil is taken to be the target leading-edge velocity distribution. In this way, the new airfoil has a realistic leading edge. This means that the user selects from the initial airfoil the approximate radius of the leading edge. The velocities at the ends of that region are called stagnation velocities (see Fig. 3, the region from A to B).
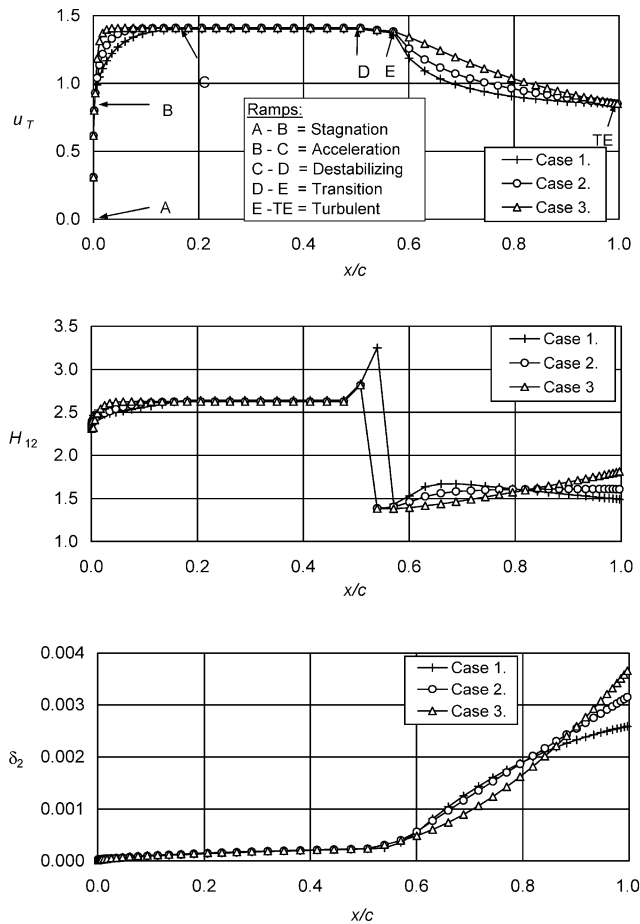
Fig. 3 Three different upper-side design velocities and corresponding boundary-layer developments at $Ma_\infty = 0.15$ and $Re = 3 \times 10^6$ (see Table 1).

Acceleration Region

The user selects the arc length of the acceleration region s_0 and the velocity at the end of the acceleration region u_0. The target-velocity distribution u_T at s_n measured downstream from the end of the stagnation region is of the form

$$u_T(s_n) = \sqrt{u_0^2 - \left(u_0^2 - u_{sT}^2\right)\left(1 - s_n/s_0\right)^A} \qquad (62)$$

where u_{sT} is the velocity at the end of the stagnation region. The parameter A determines the acceleration, and it affects the overall radii of the leading edge. Increasing the value A gradually leads to a rooftop velocity distribution (see Fig. 3, the region from B to C).

Destabilizing Region

Several problems have arisen in the development of an efficient airfoil for a low-chord Reynolds number. Boundary-layer control becomes difficult at low-chord Reynolds numbers because of the increased stability of the attached boundary layers. If the flow decelerates too early, laminar separation is common at small angles of attack. The development of a turbulent boundary layer under these conditions may depend on the formation of a transitional separation bubble. The turbulent boundary layer downstream to the separation bubble is usually thicker than that formed in an attached transition process. This will result in increased drag coefficient and may lead to a premature separation of the turbulent boundary layer. Therefore, it is highly recommended to devise methods to control the separation bubbles.

There are a few alternative approaches to this problem. Often various artificial transition-inducing devices (roughness, strips, pneumatic blowing, etc.) are used. Another way is Wortmann's idea of a destabilizing region. The velocity distribution (see Fig. 3, the region

from C to D) may be constant or have a slight adverse pressure in the region where laminar separation is expected to occur, allowing transition but avoiding separation.

On one hand, Thwaites' method includes a dimensionless gradient parameter λ for the laminar boundary-layer velocity, which predicts laminar separation when $\lambda_T < -0.090$.

On the other hand, an incompressible-flow transition should be expected when the momentum-thickness Reynolds number is

$$Re_{\delta 2} = Re\delta_2 u_T > 1.174\left(1 + \frac{22{,}400}{Re_s}\right)Re_s^{0.46} \qquad (63)$$

By applying a weak adverse pressure gradient over the long laminar destabilizing region ($0.2c - 0.3c$), the boundary-layer instability will grow without separation. Ideally, for frictional drag, the laminar-form parameter H_{12} should remain constant (≈ 3.2), and a natural transition should take place just at the steep start of the turbulent pressure region without separation. However, this kind of flow will have dangerous off-design performance, because the laminar boundary layer is very close to separation. Even a small increase in the angle of attack will cause the transition point to move quickly forward with severe results for lift and drag coefficients. Conversely, a decrease in the angle of attack causes the transition point to extend into the steep turbulent recovery region, rapidly increasing the momentum losses in the bubble. Such highly trimmed airfoils will also be very sensitive to surface waviness or roughness.

In this study, the velocity distribution of the destabilizing region is defined for a prescribed velocity-gradient parameter λ_T by Euler's step method. The velocity at point $s_n + \Delta s$ is

$$u_T(s_n + \Delta s) = u_T(s_n)\left(1 + \frac{u_T\lambda_T}{Re_{\delta 2}(s_n)\delta_2}\Delta s\right) \qquad (64)$$

The Reynolds number $Re_{\delta 2}$ based on momentum thickness is obtained from simultaneous laminar boundary-layer calculations. The user-defined velocity parameter λ_T controls how close to separation the flow is. According to Thwaites' method, the laminar form parameter is a function only of the velocity-gradient parameter, so a constant λ_T yields a constant H_{12}.

When the design Reynolds number is of the order of 10^6, the velocity-gradient parameter should be set in the range $-0.07 \leq \lambda_T \leq 0.0$ (corresponding to $2.6 \leq H_{12} \leq 3.1$) to ensure a safety margin for transition and laminar separation. Ideally, the length of the destabilizing ramp should be selected such that at the end a natural transition takes place. If the destabilizing region is too short, the abrupt pressure recovery at the beginning of the turbulent region will cause a separation bubble.

Transition/Separation Bubble Region

In low-Reynolds airfoil design ($Re < 10^6$), an active transition mechanism is used, and separation bubbles are allowed. A short ($0.03c - 0.1c$) velocity distribution can be introduced from Eq. (64) at the end of the destabilizing ramp, just steep enough ($\lambda_T < -0.090$) to ensure separation of the already destabilized laminar boundary layer. The ramp (see Fig. 3, the region from D to E) should be long enough to ensure a transition and a reattachment before the flow enters the turbulent region.

Turbulent Region

The Stratford pressure distribution[32] is widely used. It is an analytical expression for the slope of pressure recovery based on a zero skin-friction criterion throughout the region. Many airfoils using the Stratford distribution show good lift and lift-to-drag characteristics.[33,34] Their abrupt stall makes them impractical for applications with high angles of attack, because all of the recovery region may separate simultaneously.

The shape and amount of recovery-velocity distribution (see Fig. 3, the region from E to TE) in this study are defined by constant parameters K and R (Ref. 28),

$$u_T = u_r[1 + K(s_n - s_r)]^R \qquad (65)$$

Table 1 Effect of design parameters A and B ($\lambda = 0$) on drag coefficient c_d, at $Ma_\infty = 0.15$ and $Re = 3 \times 10^6$

Case	A	B	c_d (one side)
1	10	−1	0.0031
2	20	0	0.0038
3	60	8	0.0045

where u_r is the velocity and s_r is the distance at the beginning of the pressure recovery region.

In many successful sailplane profiles, Wortmann's velocity distribution is used,[35] which is a special case of Eq. (65). It yields a constant form parameter H_{12}^* and a linearly growing momentum thickness, with a derivative $\beta = d\lambda_2/ds$ when

$$R = 0.33 - \frac{0.074}{6\beta Re^{0.2}} \qquad (66)$$

and the momentum-thickness parameter is

$$K = \beta/\delta_{2r} \qquad (67)$$

The derivative β is solved iteratively to give a suitable velocity at the trailing edge. Wortmann's distribution requires that the momentum thickness δ_{2r} be known at the beginning of the pressure-recovery region.

To get more flexibility for the boundary-layer control, Wortmann's distribution is modified in this study. Then the parameters K and R are functions of the distance s_n. They are defined with a user-selected parameter, which is the second derivative of the momentum thickness $B = d\beta/ds = d^2\delta_2/ds^2$. Now the nonconstant derivative of the momentum thickness is

$$\beta(s_n) = \beta_r[1 + B(s_n - s_r)] \qquad (68)$$

where $\beta_r = (d\delta_2/ds)_r$ is the derivative of the momentum thickness at the beginning of the turbulent region. When δ_{2r} is obtained from laminar boundary-layer calculations, then for a given B and trailing-edge velocity u_{TE} the parameter β_r is solved iteratively. To produce a closed airfoil, u_{TE} can easily be found by trial and error during the design process. If B is taken positive, the velocity distribution is less concave, which produces a growing form parameter H_{12}^*. This velocity distribution has a higher drag coefficient, and on the upper side of the airfoil has a higher lift coefficient, but it is less prone to abrupt stall. If B is negative, a lower drag coefficient is obtained, and this distribution is more suitable for the lower side of the airfoil.

In Table 1, the effect of design parameters is introduced. In case 2, the parameter $B = 0$ represents Wortmann's original turbulent velocity distribution. The more concave distribution ($B = -1.0$) will cause a lower drag coefficient. However, in this case, the development of the turbulent boundary-layer-form parameter H_{12}^* will produce abrupt stalling characteristics. The combination $A = 10$ and $B = 8.0$ is appropriate for training sailplanes when mild stalling properties are preferred to a high lift-to-drag ratio.

Airfoil Thickness

In many applications the thickness of the airfoil is fixed by structural or internal volume requirements. It is therefore desirable to design the performance for a specific thickness. For angles of attack near zero, the thickness ratio is obtained from the target pressure distribution by

$$t/c \approx \frac{-0.325}{c}\sqrt{1 - Ma_\infty^2}\int_0^c (C_{p,u} + C_{p,l})\,dx \qquad (69)$$

Evaluating the Analysis Method

Evaluation of the Transition Methods

The transition methods described were tested to check their ability to predict the transition on an airfoil at different angles of attack. Reynolds number $Re = 3 \times 10^6$ was used for the NACA 0012

Table 2 Transition dependence of NACA 0012 for $\alpha = 0$ deg, $Ma_\infty = 0.1$, and $Re = 3 \times 10^6$

Method	Experimental[1,36]	Michel	e^8	e^9	e^{10}
c_d	0.0059	0.0073	0.0063	0.0061	0.0059
TrU/L	0.45c	0.34c	0.45c	0.47c	0.48c

Table 3 Transition dependence of NACA 0012 for $\alpha = 5.0$ deg, $Ma_\infty = 0.1$, and $Re = 3 \times 10^6$

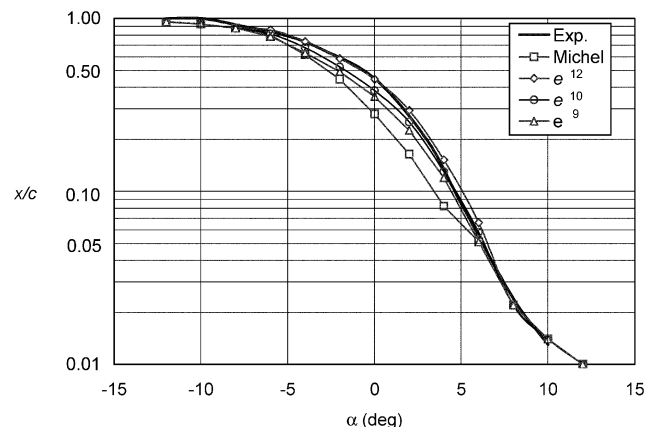| Method	Experimental[1,36]	Michel	e^8	e^9	e^{10}
c_l	0.56	0.558	0.559	0.56	0.561
c_d	0.0076	0.0086	0.0079	0.0078	0.0077
TrU	0.085c	0.082c	0.091c	0.11c	0.12c
TrL	0.79c	0.75c	0.76c	0.76c[a]	0.76c[a]

[a]Laminar separation.

Fig. 4 Transition predictions for NACA 0012 on the upper side at $Ma_\infty = 0.1$ and $Re = 3 \times 10^6$ compared to experimental data.

two-dimensional airfoil. The critical exponents $n = 8, 9, 10$, and 12 for the e^n method were tested to determine the location of the transition.

Figure 4 shows the transition predictions compared with experimental values.[36] For angles of attack higher than about 8 deg a laminar separation is detected on both sides of the airfoil. The position of a laminar separation is in good agreement with experiments. When a natural transition is detected, Michel's method predicts it slightly too early with moderate angles of attack. The best agreement was found using the e^n method with the critical exponent $n = 10$. When the critical exponent was set to $n = 12$, Fig. 4 shows that the transition was moved slightly downstream. The calculations are still in good agreement with the experiments for all angles of attack.

For evaluation of the overall transition modeling, two different angles of attack with different transition models have been used at $Re = 3 \times 10^6$. The results are shown in Tables 2 and 3.

Different transition methods have been applied in the analysis code to improve the computation of airfoil aerodynamic coefficients. In practical applications, no experimental data are generally available to optimize the transition method. Numerical results show that the locations of transition are essential factors in accurately computing the aerodynamic performance of an airfoil. Because the e^n method is based on the linear stability theory, many fundamental aspects of the transition are not taken into account. However, comparison between numerical and experimental results indicates that the e^n method combined with Thwaites' laminar separation model can successfully predict the onset point of a transition. We conclude that in the e^n model the critical exponent n for the beginning of transition is usually in the range 8–9 and for the end of the transition region n is about 10. From this position, the fully developed turbulent flow begins, and the turbulent equations are valid in the calculation model. The accuracy of Michel's method is adequate

Table 4   NACA 4412, comparison of results for $Ma_\infty = 0.18$, $Re = 4.17 \times 10^6$, and $\alpha = 12.49$ deg

Model	c_l	c_d	c_m	Separation
Calculation, no strip	1.57	0.02	−0.063	$0.82c$
Calculation, strip	1.45	0.026	−0.048	$0.74c$
Experimental	1.44	0.034	—	$\approx 0.80c$

Table 5   NACA 0012, drag coefficient comparison at $\alpha = 0$ deg and $Ma_\infty = 0.3$

Re	Transition model	c_d calculated	c_d experimental
3×10^6	strip $0.05/0.05c$	0.01	0.009
3×10^6	free $0.48/0.48c$	0.0061	0.006
6×10^6	strip $0.05/0.05c$	0.0094	0.008

for lift calculations, but the best agreement with experimental data is found with the present variant of the e^n method with the critical exponent $n \approx 10$.

NACA 4412 Airfoil

High-Lift Computations

The flow around a single-element airfoil approaching maximum lift and poststall conditions is still considered one of the most difficult computational test cases because of the extreme sensitivity of boundary-layer separations. For a low-speed test case the NACA 4412 airfoil near the stalling condition is selected. The numerical modeling of flow regimes close to the maximum lift coefficient is complicated by factors such as the unsteadiness and three-dimensionality of the flow, in addition to difficulties related to the calculating of the boundary-layer transition. In the case of NACA 4412, the computer program testing is carried out by comparing the computed results with measurements obtained by Hastings and Williams.[37] Experimental data for this airfoil were obtained in the RAE (4.0 × 2.7 m) low-speed, closed-circuit wind tunnel. The test model had a chord of 1.0 m and spanned the test section.

Wind-tunnel measurements taken for NACA 4412 at $Ma_\infty = 0.18$, $Re = 4.17 \times 10^6$, and $\alpha = 12.49$ deg (corrected) reveal a boundary-layer separation at approximately $x = 0.80c$ on the upper airfoil surface. Oil-flow visualization studies showed that the flow around the model had a two-dimensional structure up to $c_{l\,max}$. To eliminate laminar separation and to fix the boundary-layer transition, bands of height $0.28 \times 10^{-3}c$ were placed at $x = 0.014c$ and $x = 0.11c$ on the upper and lower surfaces, respectively. The experimental report indicates that the transition strips exceed the local displacement thicknesses. This results in an increase in the momentum thickness, which plays an important role in the boundary-layer development (Fig. 5). Thus, the correct prediction of starting conditions just behind the transitions is necessary for an accurate solution.

The computations were performed using 200 airfoil and 100 wake panels. The surface-pressure distribution and the boundary-layer properties are in good agreement with the measurements (Fig. 5). A spectacular improvement is obtained in the computed displacement and momentum thickness by using the strip model (see Table 4). The computed lift coefficient is in good agreement with the measured value. The drag coefficient defined from the far wake is underpredicted.

Drag-Polar Computations at $Ma_\infty = 0.15$

Calculations were performed with the free-transition model using chord Reynolds numbers of $Re = 3 \times 10^6$ and 9×10^6. A summary of the calculated and experimental results[1] is shown in Fig. 6.

The flow separation starts from the trailing edge, resulting in smooth stalling characteristics for the NACA 4412 airfoil. The maximum lift coefficient and the stalling angle of attack are well predicted by the computations. The drag coefficients are calculated with the modified Squire–Young formula and from the far wake. Both methods result in nearly identical drag coefficients for attached and
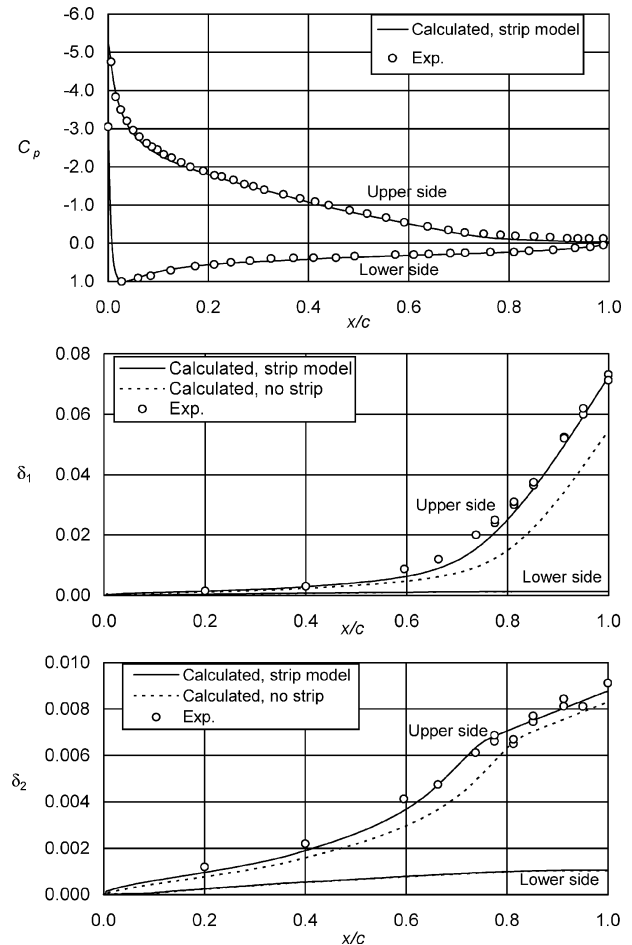

Fig. 5   NACA 4412, $Ma_\infty = 0.18$, $Re = 4.17 \times 10^6$, $\alpha = 12.49$ deg: pressure coefficient C_p, displacement thickness δ_1, and momentum thickness δ_2 compared to experimental data.
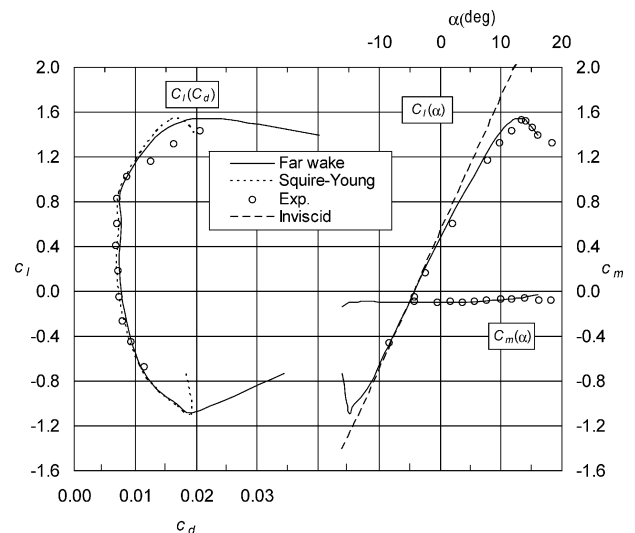

Fig. 6   NACA 4412 (free transition, $Ma_\infty = 0.15$, $Re = 3.0 \times 10^6$ calculated lift (c_l), drag (c_d) and pitching-moment (c_m) coefficients) compared to experimental data.[1]

mildly separated flows. In stall and poststall conditions, the far-wake method is in closer agreement with the experiments.

NACA 0012 Airfoil

This symmetrical 12% thick airfoil is often used in checking computer programs. It has been tested by Harris[38] over a wide range of Reynolds and Mach numbers using a model with a 0.65-m chord. The published experimental data are corrected according to
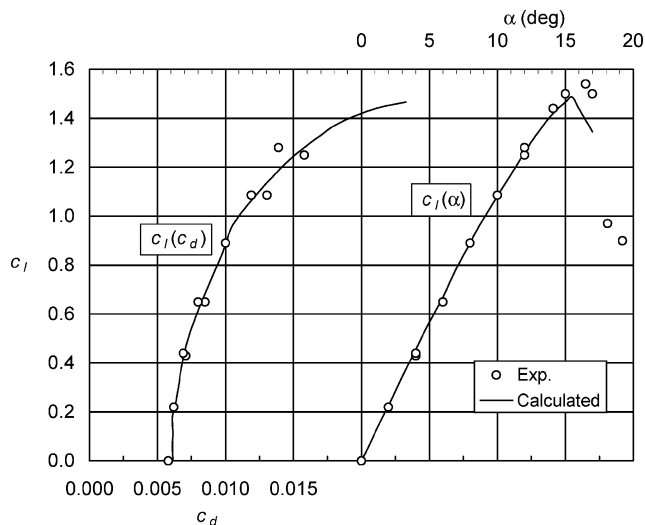
Fig. 7 NACA 0012 (free transition, $Ma_\infty = 0.1$, and $Re = 3.0 \times 10^6$: calculated lift (c_l) and drag (c_d) coefficients) compared to experimental data.[1]
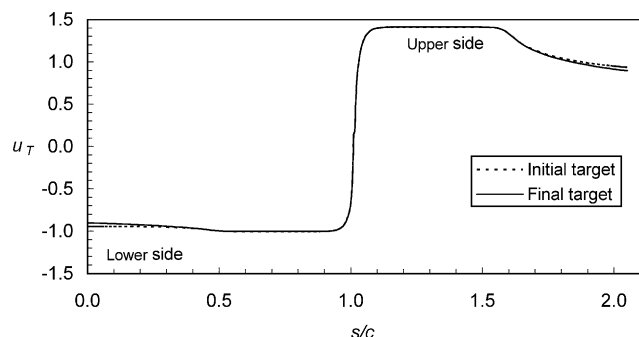

Fig. 8 Minor modifications are needed in the turbulent region of the initial target velocity to obtain a closed airfoil.

Table 6 Airfoil RP-105-066/W under the design conditions $Ma_\infty = 0$, $Re = 2.0 \times 10^6$, and $\alpha = 3.7$ deg

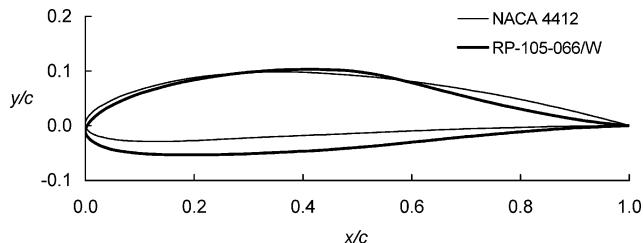| Parameter	Target	Analyzed
c_l	0.66	0.657
c_d Squire–Young	0.00629	0.00634
c_l/c_d	105	103
Transition, upper	0.51c	0.51c
Transition, lower	0.57c	0.61c

Fig. 9 Starting airfoil NACA 4412 and the new airfoil RP-105-066/W, designed from the predefined pressure distribution.
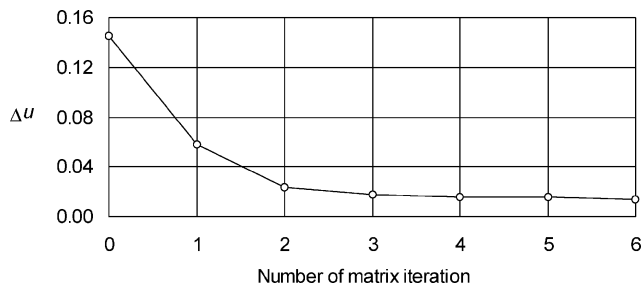

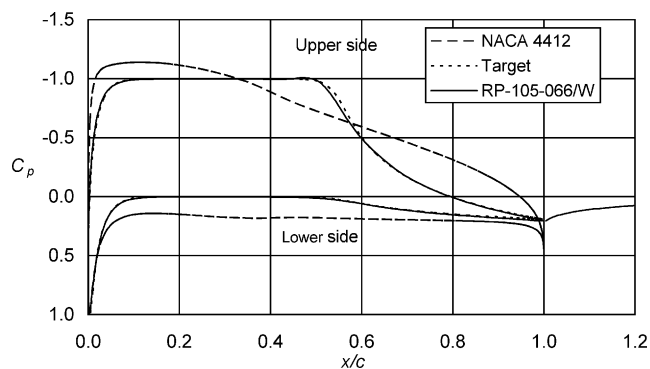Fig. 10 Convergence of the mean deviation calculated around the foil using Eq. (47).

Fig. 11 Pressure distribution of the initial section NACA 4412, the target, and obtained (RP-105-066/W) pressure distribution.

the guidelines given by Harris. The calculations were carried out with a 0.003c thick trailing edge using $200 + 100$ panels. For comparison, $Re = 3 \times 10^6$ and 6×10^6 with $Ma_\infty = 0.3$ were chosen. In the test cases, the transition point was fixed at $x = 0.05c$ on both airfoil surfaces. The same transition location was used in computations with transition-strip modeling. The height of the strip was approximated to be $0.2 \times 10^{-3}c$ for $Re = 3 \times 10^6$ and $0.1 \times 10^{-3}c$ for $Re = 6 \times 10^6$. The free transition point was determined by the boundary-layer equations using the e^{10} method (see Table 5).

In Fig. 7, the lift coefficient vs drag coefficient and lift coefficient vs angle of attack with the combined e^{10} transition and laminar-separation model are compared with experimental data up to the stall. The calculated lift and drag coefficients are in good agreement with the measured values. The stall is predicted about 2 deg too early.

Design of Airfoils

Test Case

A typical, modern, low-drag target velocity (pressure) distribution was selected to test the capabilities of the design method. On both sides of the airfoil, a short acceleration region was followed by a constant-velocity region ($0.1 < x/c < 0.5$), which destabilizes the laminar flow. For checking the accuracy of the method, their pressure coefficients were set in the design code at $C_{pu} = -1.0$ and $C_{pl} = 0.0$, respectively. Transition was induced with short separation regions. The velocities on the turbulent regions were Wortmann's distributions. Some preliminary tests were conducted to define the trailing-edge velocity for obtaining a closed airfoil (Fig. 8).

The initial geometry was an NACA 4412 airfoil section defined with the rather coarse grid of 101 coordinate points and 33 x-coordinates in the wake. The flow conditions were 3.0-deg angle of

attack, $Ma_\infty = 0$, and $Re = 2.0 \times 10^6$. Transition was free without a separation bubble. Between the first three matrix iteration cycles, the angle of attack was slightly increased to reduce the rotation of the airfoil around its trailing edge; the final angle of attack was 3.7 deg. All viscous effects were included. Six matrix inversions were done, each having 15 to 20 transpiration iterations. A large change was made from the initial wing-section geometry to obtain the new airfoil, called RP-105-066/W (Fig. 9). The history of convergence is presented in Fig. 10.

The new airfoil was analyzed under the design conditions (see Table 6). Figure 11 includes the specified and the new pressure distributions, which are practically the same.

Wind-Turbine Application

Using the present method, an airfoil was designed for wind-turbine applications for $Re = 2.0 \times 10^6$ with a target thickness of about $t/c = 0.15$. At the design point, the lift coefficient should be $c_l \approx 1.2$ with a lift-to-drag ratio greater than 120. Further

requirements include a low pitching-moment coefficient, $|c_m| <$ 0.05, to limit the structural loads. In an attempt to develop an airfoil that meets all of these requirements, a velocity distribution was generated and fine-tuned. The corresponding geometry was solved using as a starting point the NACA 4417 airfoil at 8.0-deg angle of attack with $200 + 70$ panels (airfoil and wake). Three intermediate airfoils were solved until the final airfoil RP-119-WG was obtained (Fig. 12).

The predicted thickness t/c [Eq. (69)] was 0.17, and the solved geometry had a value of 0.16. The new airfoil was tested at the
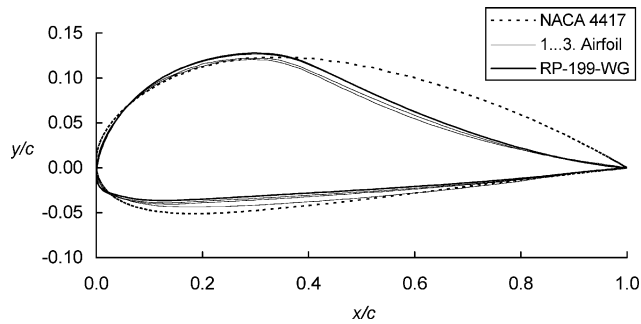

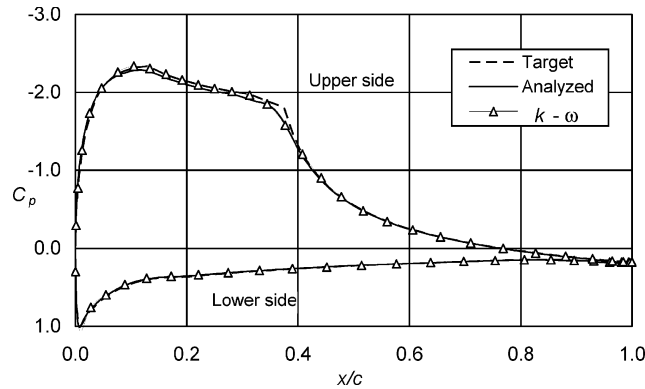**Fig. 12 Convergence history from airfoil NACA 4417 to RP-119-WG.**

Fig. 13 Pressure distribution of airfoil RP-119-WG at design conditions $Ma_\infty = 0.2$, $Re = 2.0 \times 10^6$, and $\alpha = 8.0$ deg, calculated with the present panel method (analyzed) and the Navier–Stokes method using Menter's k-ω SST turbulence model.
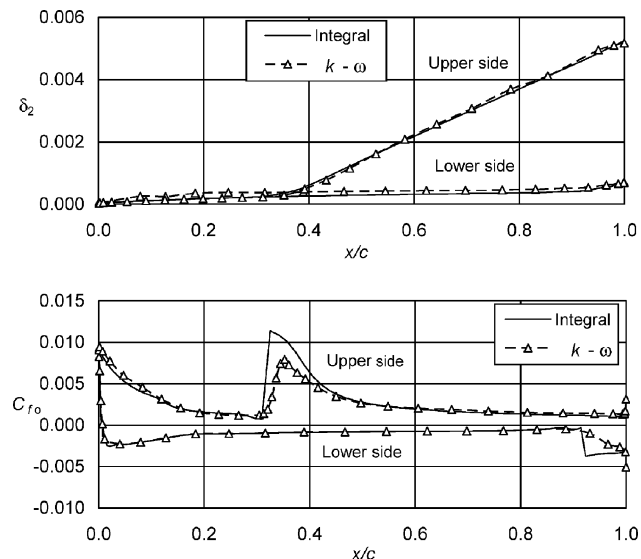

Fig. 14 Momentum thickness δ_2 and skin-friction coefficients (based on free-stream velocity) Cf_0 of airfoil RP-119-WG are calculated with the present panel method (integral) and the Navier–Stokes method using the k-ω turbulence model at design conditions $Ma_\infty = 0.2$, $Re = 2 \times 10^6$, and $\alpha = 8.0$ deg.

Table 7 Comparison of designed and analyzed properties of airfoil RP-119-WG for $Ma_\infty = 0.2$, $Re = 2 \times 10^6$, and $\alpha = 8.0$ deg

Method	c_l	c_d	c_m	Lift to drag	Transition (U/L)
Designed	1.2	0.0078	−0.021	150	0.34/0.99c (Michel)
Present analysis	1.17	0.0082	−0.02	144	0.33/0.92c (Michel)
k–ω SST[39]	1.2	0.0084	−0.02	143	0.33/0.92c (fixed)

design conditions by the present method using Michel's transition criterion and by the Navier–Stokes code FINFLO2D using Menter's k-ω turbulence model.[39]

The results are shown in Table 7. The target and analyzed pressure distributions are nearly identical, as shown in Fig. 13. A comparison of momentum thickness and skin-friction coefficients is presented in Fig. 14.

Conclusions

A new viscous-inviscid method for analyzing and designing two-dimensional single-component airfoils for subsonic speeds has been introduced and verified by numerical experiments.

The numerical method employs a panel method to represent the inviscid flow and an integral boundary-layer formulation for the viscous flow. The equations for the turbulent flow, written both in direct and in inverse form, describe attached as well as separated flows. Viscous-inviscid coupling is achieved by transpiration, and the transition criteria are included in the overall equation system.

The advanced features of the design concept are obtained by using transpiration to simulate both the viscous effects and to deform the airfoil geometry at the same time. The semi-inverse residual-correction airfoil geometry solver determines the new airfoil corresponding to a viscous target-velocity distribution by correcting the initial airfoil iteratively with transpiration. As demonstrated in the study, the airfoil can even be designed in high-lift conditions when viscous effects are significant. The design method is fast also in conventional computers, and only a few matrix iterations are needed to find the solution. The implementation of the present inverse method is possible into all existing analysis methods that utilize transpiration.

High-performance airfoils for sailplanes and windmills are designed taking into account the practical considerations. The obtained airfoil was also analyzed by a Navier–Stokes code employing the latest turbulence models. The examples confirm the ability of the present method to obtain an inverse solution with little or no discrepancy between the specified and obtained pressure distributions for a variety of cases.

Although the trend in aerodynamic calculation is toward the solution of the full Navier–Stokes equations, the computation times and costs of employing Navier–Stokes solvers remain prohibitive for many routine applications. The author believes that development of fast and economical methods, such as that demonstrated in the present study, can provide considerable improvement in efficient procedures for practical airfoil design.

References

[1]Abbot, I. A., and von Doenhoff, A. E., *Theory of Wing Sections Including a Summary of Airfoil Data*, Dover, New York, 1959.

[2]Bera, R. K., "A New Look at Theodorsen's Method in Airfoil Theory," *International Journal for Numerical Methods in Fluids*, Vol. 9, No. 3, 1989, pp. 251–262.

[3]Selig, M. S., and Maughmer, M. D., "Multipoint Inverse Airfoil Design Method Based on Conformal Mapping," *AIAA Journal*, Vol. 30, No. 5, 1992, pp. 1162–1170.

[4]Selig, M. S., and Maughmer, M. D., "Generalized Multipoint Inverse Airfoil Design," *AIAA Journal*, Vol. 30, No. 11, 1992, pp. 2618–2625.

[5]Soinne, E., "Design of Single Component Airfoils Using an Inverse Boundary Element Method," Helsinki Univ. of Technology, Lab. of Aerodynamics, Rept. 83-A2, Otaniemi, Finland, Dec. 1983.

[6]Soinne, E., and Laine, S., "An Inverse Boundary Element Method for Single Component Airfoil Design," *Journal of Aircraft*, Vol. 22, No. 6, 1985, pp. 541–543.

[7]Le Balleur, J. C., "Strong Matching Method for Computing Transonic Viscous Flows Including Wakes and Separations. Lifting Airfoils," *La Recherche Aérospatiale*, English edition, No. 3, March 1981, pp. 21–45.

[8]Accident Investigation Board Finland, "Aircraft Accident at Enontekiö on June 25, 2003," Investigation Rept. B2/2003L, Helsinki, Finland, 2005.

[9]Peltonen, R., "A Numerical Method for Analysis and Design of Airfoils in Subsonic Flow," Ph.D. Dissertation, Lab. of Aerodynamics, Helsinki Univ. of Technology, Rept. A-20, Espoo, Finland, Sept. 2000.

[10]Moran, J., *An Introduction to Theoretical and Computational Aerodynamics*, Wiley, New York, 1984, pp. 206–209.

[11]White, F. M., *Viscous Fluid Flow*, 2nd ed. McGraw-Hill, New York, 1991.

[12]Cohen, C. B., and Reshotko, E., "The Compressible Laminar Boundary Layer with Heat Transfer and Arbitrary Pressure Gradient," NACA-1294, Jan. 1956.

[13]Drela, M., and Giles, M. B., "Viscous-Inviscid Analysis of Transonic and Low Reynolds Number Airfoils," *AIAA Journal*, Vol. 25, No. 10, 1987, pp. 1347–1355.

[14]Green, J. E., Weeks, D. J., and Brooman, J. W. F., "Prediction of Turbulent Boundary Layers and Wakes in Compressible Flow by a Lag-Entrainment Method," Aerodynamics Dept., Royal Aircraft Establishment, Farnborough, Hampshire, England, U.K., R&M 3791, Jan. 1973.

[15]Lock, R. C., and Firmin, M. C. P., "Survey of Techniques for Estimating Viscous Effects in External Aerodynamics," *Proceedings of IMA Conference on Numerical Methods in Aeronautical Fluid Dynamics*, edited by P. Roe, Academic Press, New York, 1983, pp. 337–430.

[16]Howlett, J. T., "Calculation of Unsteady Transonic Flows with Mild Separation by Viscous-Inviscid Interaction," NASA TP 3197, June 1992.

[17]Cebeci, T., and Bradshaw, P., *Momentum Transfer in Boundary Layers*, McGraw-Hill, New York, 1977.

[18]Le Balleur, J. C., and Neron, M., "Computation of Viscous Flows over Airfoils Including Separation, with a Coupling Approach," AGARD CP-291, Paper 11, 1981.

[19]Melnik, R. W., Mead, H. R., and Jameson, A., "A Multi-Grid Method for the Computation of Viscid/Inviscid Interaction on Airfoils," AIAA Paper 83-0234, Jan. 1983.

[20]Mead, H. R., and Melnik, R. E., "GRUMFOIL: A Computer Code for the Viscous Transonic Flow over Airfoil," NASA CR-3806, Oct. 1985.

[21]Melnik, R. E., Chow, R. R., Mead, H. R., and Jameson, A., "An Improved Viscid/Inviscid Interaction Procedure for Transonic Flow over Airfoils," NASA CR-3805, Oct. 1985.

[22]Wolkov, A. V., and Lyapunov, S. V., "Numerical Prediction of Transonic Viscous Separated Flow past an Airfoil," *Theoretical and Computational Fluid Dynamics*, Vol. 6, No. 1, 1994, pp. 49–63.

[23]Lock, R. C., and Williams, B. R., "Estimating Viscous-Inviscid Interactions in External Aerodynamics," *Progress in Aerospace Science*, Vol. 24, No. 2, 1987, pp. 51–171.

[24]Swafford, T. W., "Analytic Approximation of Two-Dimensional Separated Turbulent Boundary-Layer Velocity Profiles," *AIAA Journal*, Vol. 21, No. 6, 1983, pp. 923–926.

[25]Michel, R., and Arnal, D., "Investigation of the Conditions for Tripping Transition with Roughness Elements and Their Influence on Boundary Layer Development," DFVLR Mitt. 84-17, 1984, pp. 103–113.

[26]Press, W. H., Flannery, B. P., Teukolsky, S. A., and Vetterling, W. T., *Numerical Recipes*, Cambridge Univ. Press, Cambridge, England, U.K., 1987, pp. 40, 41.

[27]Young, A. D., *Boundary Layers*, BSP Professional Books, Oxford, England, U.K., 1989, p. 207.

[28]Eppler, R., *Airfoil Design and Data*, Springer-Verlag, Berlin, Heidelberg, 1990, pp. 14–17.

[29]Garabedian, P., and McFadden, G., "Design of Supercritical Swept Wings," *AIAA Journal*, Vol. 20, No. 3, 1982, pp. 289–291.

[30]Malone, J. B., Narramore, J. C., and Sankar, L. N., "An Efficient Airfoil Design Method Using Navier–Stokes Equations," AGARD CP-463, May 1989, pp. 5.1–5.18.

[31]Malone, J. B., Narramore, J. C., and Sankar, L. N., "Airfoil Design Method Using the Navier–Stokes Equations," *Journal of Aircraft*, Vol. 28, No. 3, 1991, pp. 216–224.

[32]Stradford, B. S., "An Experimental Flow with Zero Skin Friction Throughout Its Region of Pressure Rise," *Journal of Fluid Mechanics*, Vol. 5, 1959, pp. 1–16.

[33]Liebeck, R. H., "A Class of Airfoils Designed for High Lift in Incompressible Flow," *Journal of Aircraft*, Vol. 10, No. 10, 1973, pp. 610–617.

[34]Liebeck, R. H., "Design of Subsonic Airfoils for High Lift," *Journal of Aircraft*, Vol. 15, No. 9, 1978, pp. 547–561.

[35]Wortmann, F. X., "Ein Beitrag zum Entwurf von Laminarprofilen für Segelflugzeuge und Hubschrauber," *Zeitschrift für Flugwissenschaften*, Vol. 3, No. 10, 1955, pp. 333–345.

[36]Gregory, N., and O'Reilly, C. L., "Low-Speed Aerodynamic Characteristics of NACA 0012 Aerofoil Section, Including the Effects of Upper-Surface Roughness Simulating Hoar Frost," NPL Aero Rept. 1308, National Physical Laboratory, Middlesex, England, U.K., Jan. 1970.

[37]Hastings, R. C., and Williams, B. R., "Studies of the Flow near a NACA 4412 Airfoil at Nearly Maximum Lift," *Aeronautical Journal*, Vol. 91, Jan. 1987, pp. 29–44.

[38]Harris, C. D., "Two-Dimensional Aerodynamic Characteristics of the NACA 0012 Airfoil in Langley 8-Foot Transonic Pressure Tunnel," NASA TM-81927, April 1981.

[39]Kaarlonen, K., "Calculation of a Wind-Generator Profile RP-119-WG at the Design Conditions," Aeronautical Engineering Dept., Helsinki Univ. of Technology, Espoo, Finland, 2000 (in Finnish, unpublished).